JOURNAL OF MAGNETIC RESONANCE IMAGING 19:6–18 (2004)

Invited Review

Clinical Applications of Diffusion Tensor Imaging

Qian Dong, MD, Robert C. Welsh, PhD,* Thomas L. Chenevert, PhD, Ruth C. Carlos, MD, MS, Pia Maly-Sundgren, MD, PhD, Diana M. Gomez-Hassan, MD, PhD, and Suresh K. Mukherji, MD

Directionally-ordered cellular structures that impede water motion, such as cell membranes and myelin, result in water mobility that is also directionally-dependent. Diffusion tensor imaging characterizes this directional nature of water motion and thereby provides structural information that cannot be obtained by standard anatomic imaging. Quantitative apparent diffusion coefficients and fractional anisotropy have emerged from being primarily research tools to methods enabling valuable clinical applications. This review describes the clinical utility of diffusion tensor imaging, including the basic principles of the technique, acquisition, data analysis, and the major clinical applications.

Key Words: diffusion tensor; MRI; DTI; brain; apparent diffusion coefficient; diffusion anisotropy
J. Magn. Reson. Imaging 2004;19:6–18.

DIFFUSION TENSOR IMAGING (DTI) relies on thermally-driven random motion of water molecules to supply microscopic structural information in vivo (1,2). Random motion of water molecules, also known as Brownian motion, can be quantified and reflects intrinsic features of tissue microstructure in vivo (3). In unconstrained water molecules in a pure liquid environment free of impediments or in a sample where the barriers are not coherently oriented as in a cyst, diffusion is equal in all directions. This situation is referred to as "isotropic." In brain tissue, however, water diffusion is substantially reduced by impediments placed by structures such as myelin sheaths, cell membranes, and white matter tracts. In general, the diffusion of the water molecules is less restricted along the long-axis of a group of aligned tissue fibers (such as those of white matter) than perpendicular to it. The condition of directionally-dependent diffusion is referred to as "anisotropic." Three descriptive levels are commonly used to portray tissue diffusion properties. First, the apparent diffusion coefficient (ADC) can be quantified to provide information on the degree of restriction of water molecules. Second, the degree of directionality is often described via an index such as fractional anisotropy (FA). Highly-directional axonal fibers, such as white matter, are revealed as hyperintense on an FA map. Third, the predominant diffusion direction can also be determined, which is used as an input to fiber tracking algorithms. In general, the more unrestricted the water molecules are in a given tissue, the higher the ADC will be and the lower the anisotropy will be. Directionally-encoded color (DEC), another method to identify major fiber direction, recently developed by Pajevic and Pierpaoli (4), derives additional information from DTI. The location and orientation of major white matter fiber tracts can be revealed by hue with these full tensor-based color methods. With recent improvements in MR hardware, DTI acquisition times have been reduced to allow complete brain coverage in a clinically acceptable period. These features of the DTI technique provide a sensitive means to identify different components of brain tissue and evaluate the integrity and direction of the fiber tracts in various pathological conditions. Tissue maladies studied by DTI include cerebral ischemia, multiple sclerosis, epilepsy, metabolic disorders, and brain tumor.

PHYSICS, ACQUISITION, AND DATA ANALYSIS

Diffusion, Scalar, and Anisotropic

Tensor imaging is predicated on the self-diffusion of water in vivo and how free-isotropic self-diffusion may be affected by the properties of the tissue. Diffusion, also referred to Brownian Motion, is the inherent random motion of a molecule due to its thermal energy. Self-diffusion was first observed by Brown in 1827 (5), and quantified by Einstein in 1905 (6). In a liquid, diffusion is determined by the size and temperature of the molecule and the viscosity of the medium. On average, there is no net change in position over an ensemble of water molecules since there is no preferred migration direction. Each molecule, however, will randomly move about, and will have a net root mean square displacement (RMS). Along any given direction, the RMS displacement is given by

$$\mathrm{RMS} = \sqrt{2D\Delta} \qquad (1)$$

Department of Radiology, University of Michigan, Ann Arbor, Michigan.
*Address reprint requests to: R.C.W., University of Michigan Medical Center, Department of Radiology-MRI Division, 1500 E. Medical Center Drive, Ann Arbor, MI 48109-0030. E-mail: rcwelsh@umich.edu
Received May 13, 2003; Accepted August 22, 2003.
DOI 10.1002/jmri.10424
Published online in Wiley InterScience (www.interscience.wiley.com).

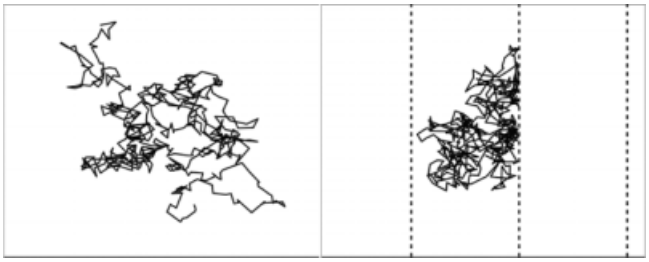

Figure 1. Both panels illustrate the random motion of a single water molecule due to diffusion for 60 msec. The left panel demonstrates free diffusion, while in the right panel the molecule is constrained by the vertical boundaries indicated by the dashed lines.

where Δ is the time the molecule diffuses, and D is the diffusion coefficient. Essentially, during a time interval Δ, a water molecule "samples" its local environment. In an isotropic medium, such as a water bath at a constant temperature, the water molecules that are away from any boundary will isotropically diffuse. This isotropic diffusion can be made anisotropic by the introduction of boundaries. If the boundaries are highly impermeable, the water will be strictly bounded and diffusion will take place mainly along the direction parallel to the boundary. However, if this boundary is permeable, molecules will traverse boundaries, although the RMS displacement in this direction is reduced compared to parallel to the boundaries. Effectively, two diffusion coefficients $D_{\parallel}$ and $D_{\perp}$, one for random motion parallel and one for random motion transverse to the boundary result in an anisotropy of the diffusion coefficient ($D_{\perp} \neq D_{\parallel}$).

Examples of free and bounded diffusion are shown in Fig. 1. Microscopically, the intrinsic diffusion coefficient is still the same, however the observed diffusion coefficient is reduced as the boundary becomes impermeable.

Note that if the diffusion time is insufficient, then the boundaries, permeable or not, will not be probed by the water molecules and any difference in diffusion coefficients will not be detected.

Diffusion Tensor

Under more general conditions, the diffusion properties are no longer limited to being scalar in nature (i.e., isotropic), and the diffusion coefficient can be elevated to a tensor form (7–9).

$$D \rightarrow \hat{D} = \begin{pmatrix} D_{xx} & D_{xy} & D_{xz} \\ D_{yx} & D_{yy} & D_{yz} \\ D_{zx} & D_{zy} & D_{zz} \end{pmatrix} \tag{2}$$

In tensor form, the diffusion coefficient can now have three principal values (D_{xx}, D_{yy}, and D_{zz}). Additionally, if the measurement axes do not correspond to the natural symmetry axes of the object being measured, the tensor will take a nondiagonal form and crossterms will appear (D_{xy}, D_{xz}, and D_{yz}). Due to symmetry properties of diffusion, there are only six independent terms in the tensor ($D_{xy} = D_{yx}$, $D_{xz} = D_{zx}$, and $D_{yz} = D_{zy}$).

Nuclear Magnetic Resonance Acquisition

Scalar diffusion measurements are made by using a pair of pulsed magnetic field gradients (10). Using a displacement-encoding scheme as shown in Fig. 2, the spin-echo amplitude A as compared to the echo amplitude A_0 without diffusion gradients is given by the following equation:

$$A = A_0 e^{-D\gamma^2 G^2 \delta^2 (\Delta - \delta/3)} \tag{3a}$$

$$A = A_0 e^{-bD} \tag{3b}$$

where Δ is the diffusion time, γ is the proton gyromagnetic ratio, δ is the encoding gradient pulse width, G is the gradient strength, and the quantity of interest D is the diffusion coefficient. During the first gradient, the current position of the molecule is encoded with phase. The second gradient then will rewind phase with a net phase resulting from any net displacement due to random motion. Due to the incoherent nature of random motion, the residual phase of the water molecules will be uncorrelated, resulting in signal degradation as given by Eq. [3]. Note that the diffusion coefficient measured here is a scalar quantity that is sufficient to describe diffusion only if the system exhibits isotropic diffusion. The diffusion gradient timing and strength is summarized in Eq. [3b] as the "b" factor, $b = \gamma^2 G^2 \delta^2 (\Delta - \delta/3)$.

DTI

With the tensor description, there are now six unknown quantities that must be determined, as compared to a single diffusion coefficient for isotropic media. Since the diffusion coefficient is elevated to the status of a tensor (matrix), the b-factor must be as well, and Eq. [3b] now takes the form

$$A = A_0 e^{-\hat{b}\hat{D}} \tag{4a}$$

where

$$\hat{b}\hat{D} = \sum_i \sum_j b_{ij} D_{ij} \tag{4b}$$

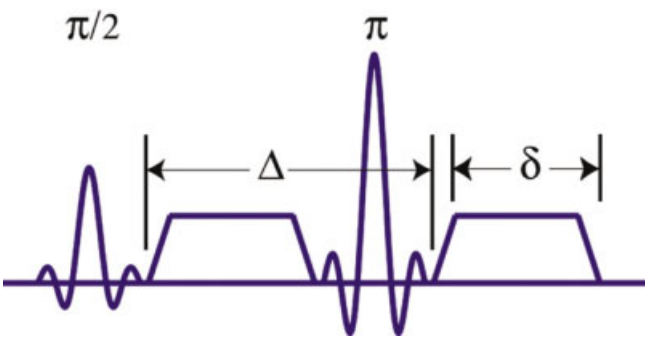

Figure 2. Stejskal/Tanner diffusion preparation: initial 90° RF pulse, followed by first diffusion lobe, 180° refocusing RF pulse, then second diffusion lobe. Leading edges of diffusion lobes are separated by Δ. Each lobe has duration δ.

and in the case of rectangular gradient pulses the *b*-matrix takes the simplified form of

$$b_{ij} = \gamma^2 G_i G_j \delta^2 (\Delta - \delta/3) \quad (4c)$$

For more complex diffusion gradient waveforms a numerical solution for the *b*-matrix must be calculated (11,12).

A minimum of seven diffusion-weighted images are acquired (gradient directions are noncolinear) (13) to solve for the tensor components of diffusion, D_{ij}, in Eq. [4a]. As a result, each voxel of the image then has a diffusion tensor defined. By applying a mathematical operation known as diagonalization, the eigenvalues (of which there will be three: λ_1, λ_2, and λ_3) and eigenvectors (again three: ϵ_1, ϵ_2, and ϵ_3) of the tensor can be determined. The largest of the three eigenvalues (which are diffusion coefficients themselves) is the value of the maximal diffusion, regardless of direction. The corresponding eigenvector for this maximum eigenvalue points in the direction of maximal diffusion. This direction is parallel to the boundaries that give rise to anisotropy in the system. Two identical samples of tissue randomly oriented with respect to each other will have the same eigenvalues calculated from the diffusion tensor. The samples will only differ in the resulting eigenvectors. Figure 3 illustrates a simple numerical simulation of anisotropic diffusion and the resulting principal eigenvectors are displayed on each pixel of a four by three image. In the figure, pixels of identical tissue samples lie in the same column, differing only in orientation. Increasingly more anisotropic tissue is simulated and illustrated left to right in the figure.

MRI Acquisition

One of the primary difficulties of imaging is patient/subject motion. This is particularly true for diffusion-weighted imaging in which diffusion-sensitization pulses amplify bulk motion phase artifact. To mitigate motion artifact, most diffusion imaging sequences are based on single-shot echo-planar imaging (EPI). Recently, spiral imaging has also been used in diffusion imaging (14). If multishot imaging is done, it is paramount that navigation echoes are acquired to correct for phase discontinuity between shots (15,16). Both single-shot EPI and spiral acquisition suffer from magnetic susceptibility artifact, though less in spiral acquisition due to the nature of the trajectory through k-space (17). Improvements in image resolution and reduction of distortion have been made using PROPELLOR and SENSE-EPI techniques (18,19).

To solve for the diffusion tensor $\hat{D}$, at least seven diffusion-weighted images are required, though more acquisition will improve signal to noise ratio (SNR). In particular, to provide the minimum bias in determination of tensor components, the gradient vectors are distributed spatially on a unit sphere according to a model of how electric charge distributes itself to minimize interaction energy (20,21).

Gradients short in duration, but large in amplitude, are best for diffusion imaging. A ramification of such a diffusion-gradient scheme is the rise of eddy currents, which greatly affect imaging techniques such as EPI and spiral. One method of mitigating large gradient switching is to use a twice-refocused spin-echo technique proposed by Reese et al (22). Additionally, gradient pre-emphasis can be used (23).

DTI Metrics and Presentation

DTI provides a very rich dataset that requires some form of data reduction for a more interpretable presentation. It is important that any scalar metric formed from the eigenvalues of the diffusion tensor be "rotationally invariant," i.e., the scalar metric is independent of the orientation of the gradient axis direction and the eigenvalue sorting order (24). Isotropic diffusion is well characterized by the trace of the diffusion tensor

$$\mathrm{Tr}(\hat{D}) = \lambda_1 + \lambda_2 + \lambda_3 \quad (5)$$

The trace, or one-third of the trace (i.e., the mean of the eigenvalues), is also an important scalar metric for anisotropic media, since it represents the average diffusivity of the media. Typically, this quantity is referred to as the ADC. Since the trace is scalar invariant, one need not determine the full tensor to measure ADC; the sum of the diffusion coefficients measured along any three orthogonal directions is sufficient to measure the trace or the ADC. However, more importantly for the clinical application of the investigation of white-matter integrity, metrics of diffusion anisotropy are more appropriate. Two very useful metrics are FA, which is a measure of the portion of the magnitude of the diffusion tensor due to anisotropy,

$$\mathrm{FA}(\hat{D}) = \sqrt{1/2}\,\frac{\sqrt{(\lambda_1-\lambda_2)^2 + (\lambda_2-\lambda_3)^2 + (\lambda_3-\lambda_1)^2}}{\sqrt{\lambda_1^2+\lambda_2^2+\lambda_3^2}} \quad (6)$$

and relative anisotropy (RA), derived from a ratio of the anisotropic portion of the diffusion tensor to the isotropic portion,

$$\mathrm{RA}(\hat{D}) = \frac{\sqrt{(\lambda_1-\lambda_2)^2 + (\lambda_2-\lambda_3)^2 + (\lambda_3-\lambda_1)^2}}{\mathrm{Tr}(\hat{D})} \quad (7)$$

Both anisotropy indices, which are dimensionless but quantitative, acquire a value of 0.0 for a purely isotropic medium. For a highly anisotropic, cylindrically symmetric medium ($\lambda_1 > \lambda_2 = \lambda_3$) FA tends towards 1, while RA tends towards $\sqrt{2}$. Both FA and RA maps can be presented as gray scale images for evaluation.

Another form of data presentation is the combination of the eigenvalue information into a color image. By choosing the eigenvector (ϵ_1) associated with the largest eigenvalue, the principal diffusion direction of the underlying brain structure can be encoded with color and the magnitude of the anisotropy, such as FA, can be further used as an illumination factor of the calculation of a directionally encoded color image (4). This results in a calculation of the color components (R, G, and B) of a pixel given by:

$$\mathrm{R} = \mathrm{FA}|\varepsilon_x^1|,\ \mathrm{G} = \mathrm{FA}|\varepsilon_{iy}^1|,\ \mathrm{B} = \mathrm{FA}|\varepsilon_z^1| \quad (8)$$

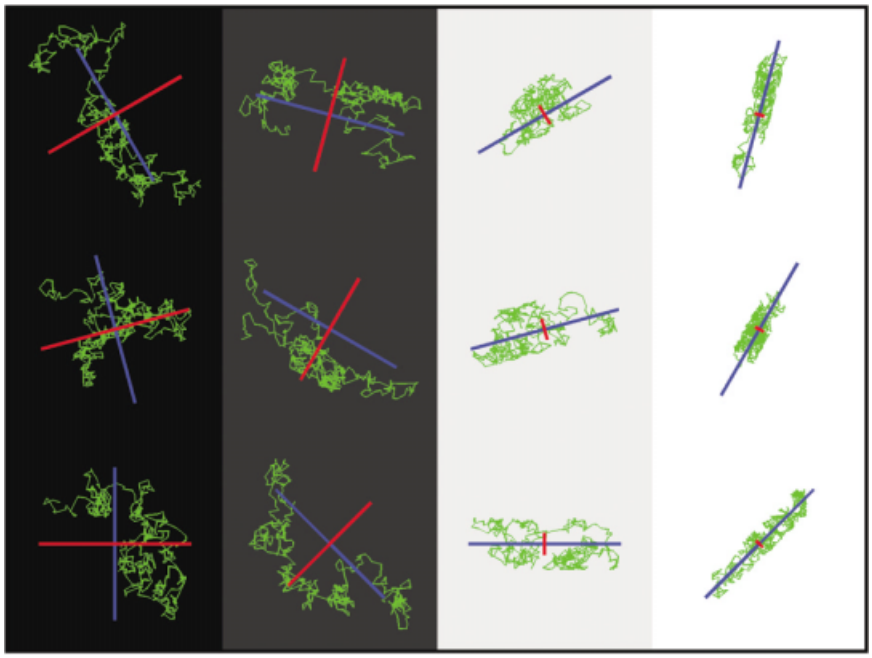

Figure 3. A graphical illustration of a Monte Carlo diffusion simulation for a 4 × 3 pixel image. The simulated tissue has impermeable boundaries, which give rise to anisotropy, oriented at a slowly increasing angle ($\pi/12$ increment per pixel, increasing bottom to top, left to right). The resulting principal eigenvector, which is along the direction of maximal diffusion, is indicated by the blue line present on top of each random walk shown in green (a single particle is shown for clarity). The secondary eigenvector is shown in red. The length of each eigenvector is indicative of the corresponding eigenvalue. Finally, the background image is the fractional anisotropy (FA) map calculated from these eigenvalues. Black indicates little or no anisotropy, while white is FA = 1. The boundary spacing is wide, giving a vanishing anisotropy in the leftmost column of pixels and decreasing to the right, resulting in higher values of anisotropy. For a given value of anisotropy, the only thing changing while moving up is the orientation of the principal diffusion. The major eigenvalue is the same throughout the image, while the second eigenvalue (length of red line) changes as the boundary spacing decreases.

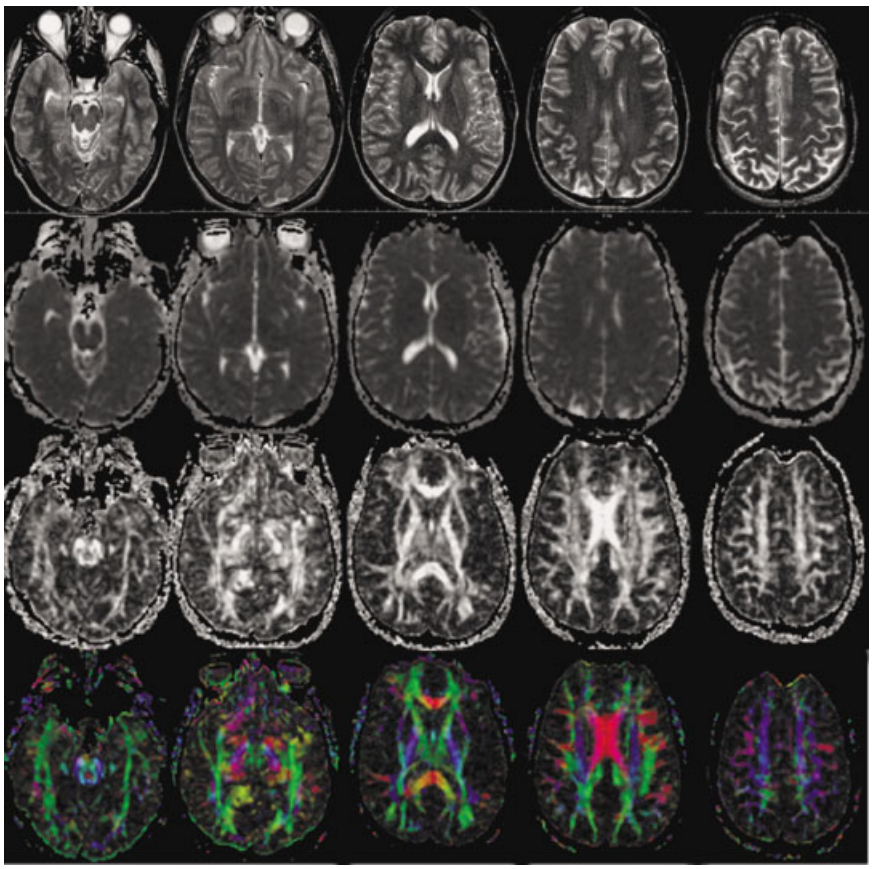

Figure 4. Axial multisection T2-weighted (first row), ADC map (second row), and FA map (third row) images from a normal volunteer with a DTI technique, obtained using a single shot spin echo EPI sequence. ADC and FA maps were generated with vendor-provided software. Highly directional white matter structures are sensitively demonstrated on FA maps. DEC images (bottom row) indicate superior–inferior (SI) fiber orientation as blue, anterior–posterior (AP) fiber orientation as green, and left–right (LR) fiber orientation as red. Fibers along directions other than these are demonstrated by a proportional mix of RGB according to the vector components along their principal directions (SI, AP, LR).

Fiber Tractography

Working from the assumption that white matter tract direction can be measured with diffusion tensor imaging, the field of fiber tractography addresses the possibilities of noninvasive digital reconstruction of neuronal connectivity (25,26). The general concept is that in each voxel, the local fiber orientation is measured through diffusion tensor imaging. The task of tractography is to sensibly assign mathematical associations between adjacent voxels based on eigenvalue and eigenvector information. A variety of fiber-tracking algorithms have been introduced and are beyond the scope of this review (27). These methods hold the promise of allowing full reconstruction of white matter tracts that connect distal regions of gray matter. However, a major challenge to fiber tracking is what happens when fiber bundles cross or coexist in single voxels.

Crossing Fibers

Crossing fibers are not captured in the mathematical model of a diffusion tensor and can appear as a voxel of low anisotropy (28). This can result in the breakdown of a fiber trajectory. Solutions to this problem have been proposed that are sensitive to multiple fiber directions in a single voxel, but these require much larger diffusion-weighted datasets, nearly 50 in the case of high angular resolution diffusion (29,30), and hundreds of diffusion images in the case of diffusion spectrum imaging (31). Investigations to address stability and performance of complex fiber configurations are underway, but are beyond the targeted scope of this review.

Sample MR Protocols and Imaging Processing

In addition to a standard anatomical imaging protocol which includes routing T1-weighted, T2-weighted, fluid-attentuated-inversion recovery (FLAIR) and, frequently, contrast-enhanced T1-weighted sequences, diffusion tensor imaging was obtained using a single shot spin-echo EPI technique along nine different directions with a b value of 1000 seconds/mm^2 in our institution. All examinations use a 1.5-T system with the manufacturer-supplied birdcage, quadrature head coil.

Image postprocessing is performed to generate ADC and FA maps with vendor-provided software (Fig. 4). Initially, images are preprocessed to remove image distortion that arises from the EPI readout: shear, compression, and shift are corrected. To further reduce artifactual values, a noise threshold is applied. Finally, a tensor dataset for each voxel (including eigenvalues and eigenvectors) is generated. DEC FA-weighted images are calculated according to the scheme by Pajevic and Pierpaoli (4).

CLINICAL APPLICATIONS

Normal Brain Maturation and Aging

Normal human brain maturation begins in utero and continues after birth into adolescence, with the most dramatic changes in myelination in the first few years of life. Characteristic MRI signal changes on T1- and T2-weighted images may reflect a decrease in brain water content and an increase in white matter myelination during brain maturation in children. Quantitative analysis with newer techniques provides more information in assessing brain maturational process than conventional MR imaging sequences. The properties of DTI in investigating movement of water molecules and microstructures of the cerebral tissue permit a sensitive imaging modality to assess brain maturation in children, newborns, or premature infants. Previous studies have shown that the ADC decreases and the diffusion anisotropy increases with increasing gestational age in some white matter regions (32,33). This observation of decreasing ADC and increasing FA continues into childhood and adolescence (Fig. 5) (34,35). Such findings have been shown to correlate with decreasing total water content, as well as progressing myelination and increasing organization of white matter fiber tracts. Failure to follow these normal developmental changes in water diffusion may be an early marker of brain injury in newborns (36).

In addition to the maturation studies, DTI has been also used in normal aging to detect age-related degeneration (37–39). Cerebral white matter has shown age-related ADC elevation in adults older than 40 years of age (40). A decrease in diffusion anisotropy has been found to occur after 20 years of age (Fig. 6). These results, however, may indicate underlying physiologic processes, such as loss of myelin and axonal fibers and increased extracellular space that occurs in normal aging.

Cerebral Ischemia

Cerebral ischemia occurs when blood vessels carrying oxygen and other nutrients to a specific part of the brain are occluded or damaged. A cascade of biochemical mechanisms is triggered within the ischemic tissue when cerebral blood flow decreases below 10–15 mL/100 g/minute. As a result of this rapid failure of high-energy metabolism, an influx of water from the extracellular compartment causes the cell to swell, termed cytotoxic edema (41). Early diagnosis is crucial for effective therapy in the setting of acute ischemia, since some tissue remains viable if perfusion is reestablished quickly. In spite of technical advances in conventional MRI and CT, ischemic parenchymal lesions in the early stages are poorly assessed. With conventional MR techniques, the ischemia could only be demonstrated at a later stage, when disruption of the blood–brain barrier has already led to water and macromolecule exudation from the vascular circulation, leading to accumulation of fluid in the damaged tissue (vasogenic edema). Diffusion-weighted imaging and the diffusion tensor techniques have been extensively used to reliably detect acute ischemic brain injury when conventional MR imaging is still normal (42–44). Moreover, its ability to distinguish acute from chronic in the course of ischemic changes may lead to enhanced clinical care.

In the acute phase, ADC is initially reduced by approximately 30% to 50% within 30 minutes after onset of focal ischemia (45–49) (Fig. 7). Pseudonormalization of decreased ADC value occurs approximately seven days after the event, and is followed by a subsequent ADC increase, as ischemia enters the chronic phase in which cytotoxic edema develops (Fig. 8). Due to heter-

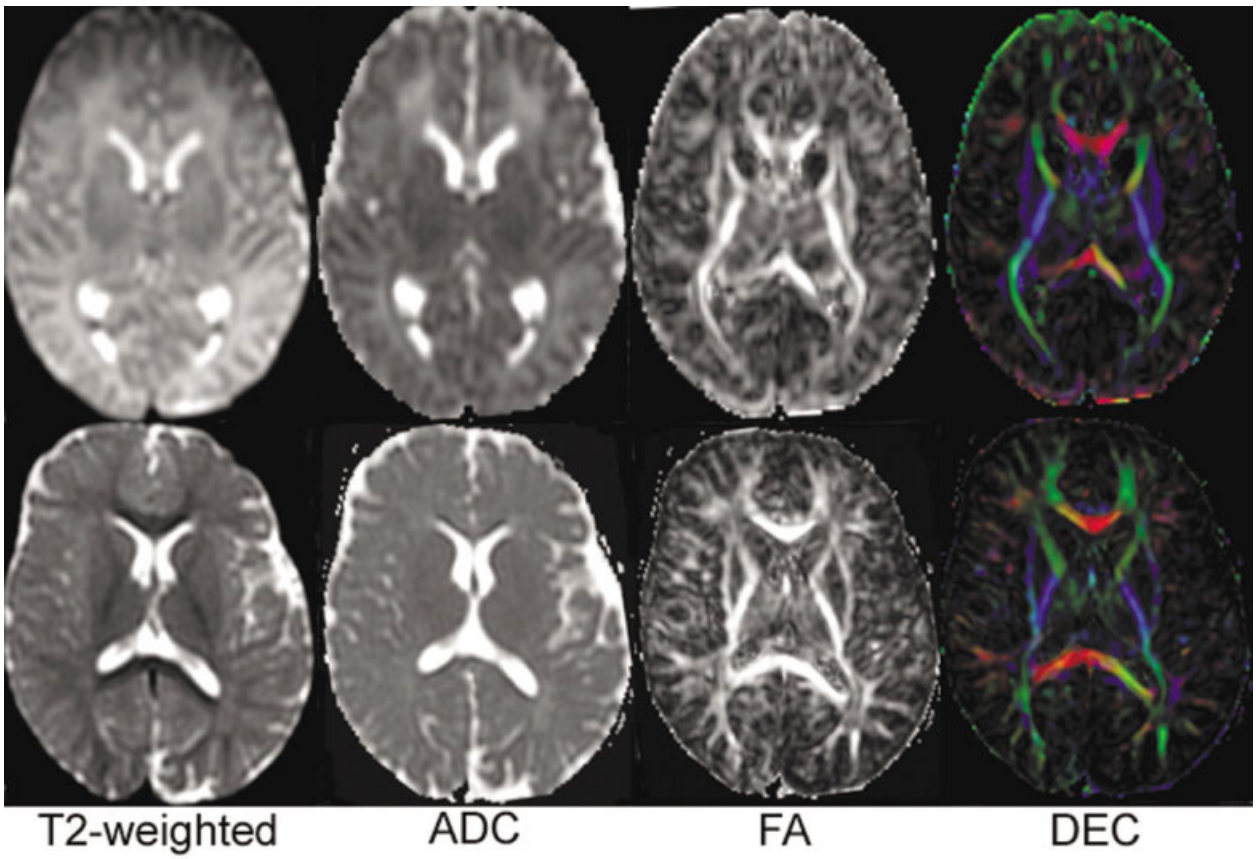

Figure 5. T2-weighted images, ADC, FA, and DEC maps of a three-day-old boy (top row) and a one-year-old boy (bottom row) without brain abnormalities on clinical MRI. During the first year of brain maturation, the white matter signal decreases on T2-weighted images; the ADC map has less gray–white matter contrast, with markedly decreased ADC value in white matter; development of central and peripheral white matter structures are identified with increasing anisotropy on FA and DEC maps.

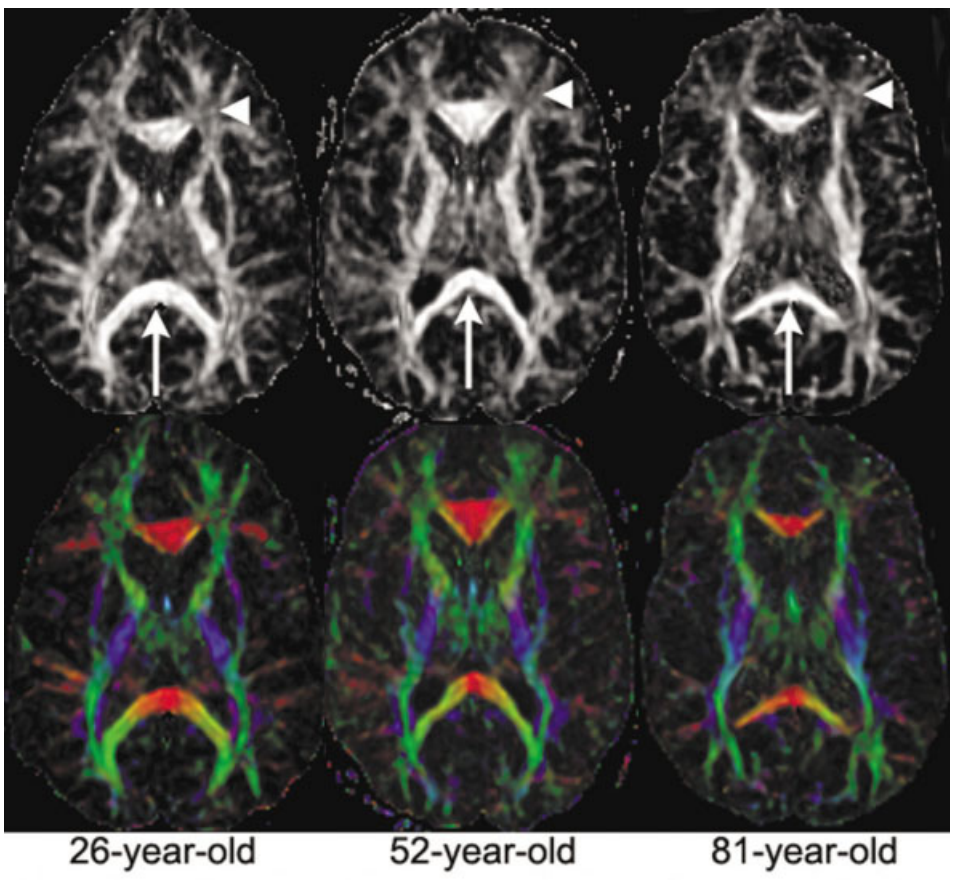

Figure 6. FA and DEC maps obtained from three adults with normal conventional MRIs show age-related white matter degeneration in the corpus callosum (arrows) and the subcortical frontal white matter (arrowheads).

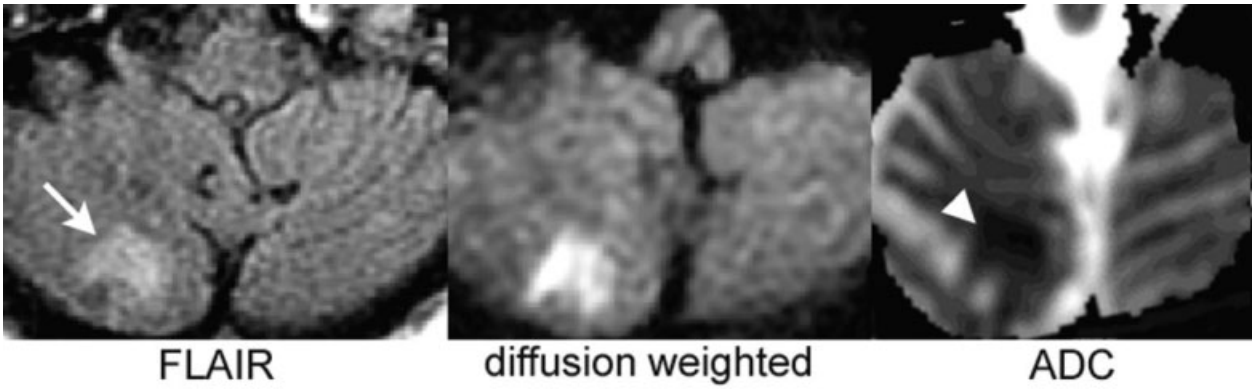

Figure 7. Axial images obtained in an 86-year-old woman 48 hours after stroke onset show a lesion (arrow) in the right cerebellum with high signal intensity on the FLAIR image, which can easily be seen on the diffusion weighted image. This acute ischemic change is confirmed by decreased ADC on the ADC map (arrowhead).

ogeneity of the ischemic process, more severe ADC reduction in white matter than in gray matter has been demonstrated during acute and early subacute ischemia (50). In addition to substantial changes in ADC value, an acute elevation in FA has been also observed in ischemic white matter but not in ischemic gray matter, followed by a significant reduction in FA during the chronic phase of cerebral ischemia (51). These changes are thought to be due to loss of organization in normal structures when the cytoarchitecture is disrupted. In addition to providing information regarding the course of ischemia, ADC threshold values have shown to be useful in predicting tissue viability and stroke outcome (47). These powerful features of the DTI technique yield unique insights into ultrastructural changes of stroke evolution, which are not available with conventional MRI.

Wallerian degeneration (WD) refers to antegrade degeneration of axons and their myelin sheaths as a result of proximal axonal injury or death of the cell body. The corticospinal tract is most commonly involved, due to cerebral infarction occurring ipsilaterally. T2 signal intensity abnormalities in the degenerating tract can be identified with conventional MRI within 4–10 weeks after acute insult (52). Recently, several studies (53–56) have shown severely reduced diffusion anisotropy and increased ADC in WD by using the MR diffusion technique. The mechanism responsible for these changes is considered to be axonal loss after ischemic or hemorrhagic stroke. Pierpaoli et al (56) demonstrated that DTI is more sensitive than T2-weighted imaging in detecting WD, and has the potential to distinguish primary stroke lesions from the areas of WD (Fig. 9). While diffusion anisotropy is reduced in both the primary lesion and the areas of WD, ADC is only slightly increased in WD, while it is greatly increased in the primary lesion.

Multiple Sclerosis

MRI has been considered to be the most informative noninvasive method to diagnose and monitor disease progression in patients with multiple sclerosis (MS) (57). However, conventional T2-weighted MR images do not sufficiently correlate with histopathological substrates and clinical disability (57). Conventional T2-weighted images are unable to distinguish underlying histopathological substrates, such as inflammation, edema, demyelination, gliosis, and axonal loss, because all of the above lesions have identical high signal on T2-weighted images. Moreover, T2-weighted images can not detect occult tissue damage within normal appearing white matter (NAWM), which may contribute to the disability of patients with MS. DTI offers quantitative information complementary to that provided by other MR techniques in evaluating the structural damage occurring in MS lesions and NAWM (58–68).

Recent studies (58–69) have demonstrated that: 1) lesions had higher ADC and lower FA than NAWM, and higher ADC and lower FA values in patient NAWM than that from normal control subject white matter (Table 1). 2) A significantly increased ADC and decreased FA were found in acute (enhancing) vs. MS lesions compared to chronic (nonenhancing) lesions. 3) Nonenhancing T1-hypointense lesions had higher ADC and lower FA values compared to T1-isointense lesions. 4) ADC was significantly higher in patients with secondary progressive MS than in patients with primary progressive MS (67,69). 5) FA values were more sensitive than ADC values in detecting white matter abnormalities in MS (58,61,66). All these findings may reflect a net loss and disorganization of structural barriers to water molecular motion (Fig. 10). Bozzali et al (68) also found increased water diffusivity in the cerebral gray matter (GM) of patients with MS, suggesting cerebral GM is not spared by the MS pathologic process.

Epilepsy

Epilepsy is a common neurological disorder characterized by recurrent seizures due to abnormal electrical discharges in the brain. It is estimated that 20% of patients with epilepsy are refractory to all forms of medical treatment (70). Surgical resection of epileptogenic structural disorders such as mesial temporal sclerosis, tumors, and vascular malformations may improve the quality of life by achieving complete or maximal seizure control without adding neurological deficit in patients with medically intractable epilepsy. Complex partial seizure, the most common type of refractory epilepsy, frequently involves the temporal lobe. Mesial temporal sclerosis or hippocampal sclerosis is a common pathol-

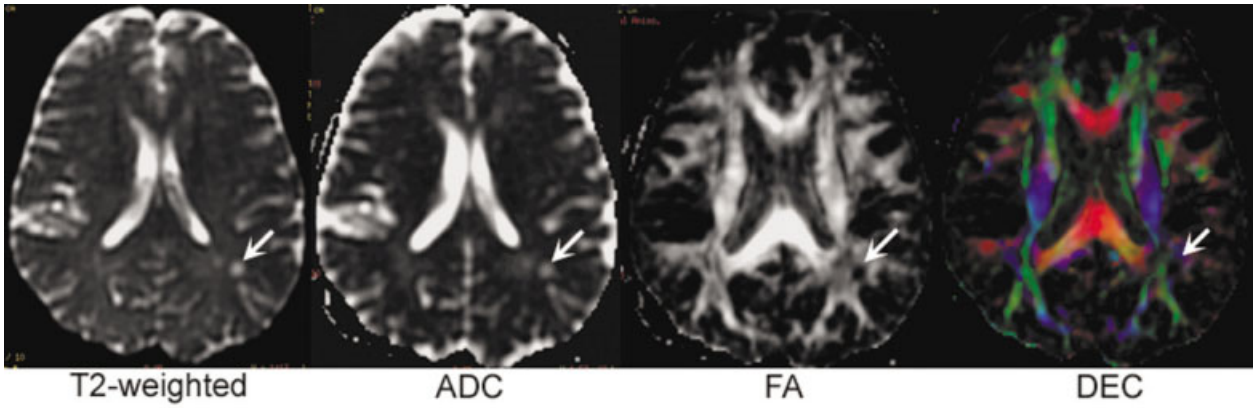

Figure 8. Axial images in a 59-year-old female with a history of chronic cerebral ischemia showing the abnormal increased T2 signal (arrow) on the T2-weighted image. There is an increased ADC value (1.13×10^{-9} mm^2/second) compared to the contralateral analogous region (0.78×10^{-9} mm^2/second). In the FA map and the DEC image, the white matter in the area of lesion (arrows) shows a decrease in fractional anisotropy.

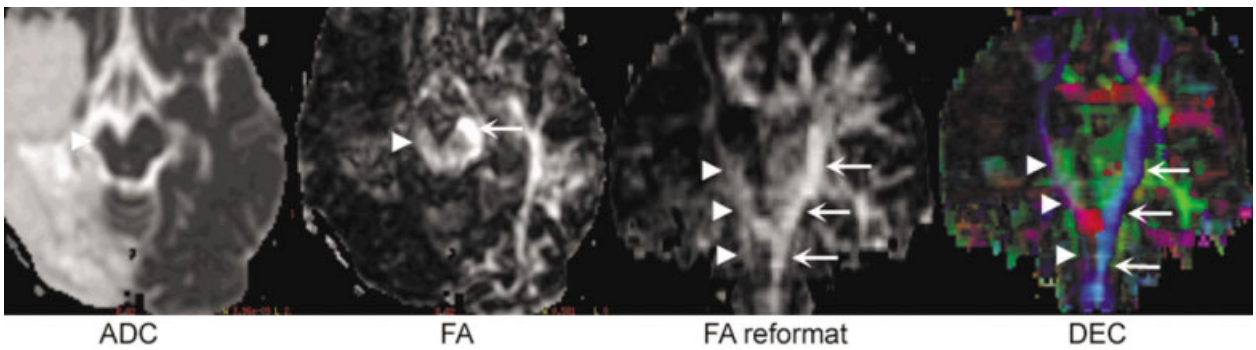

Figure 9. Axial images in a 14-year-old female who suffered a left middle cerebral artery stroke. the ADC map, FA map, reformatted FA map, and DEC image indicate that the right corticospinal tract (arrowheads) ipsilateral to the infarct is atrophic and that anisotropy is lower than on the opposite side (arrows).

Table 1
MD and FA Values in MS Studies

Reference	Year	*N* (patients/controls)	MD ($\times 10^{-9}$ mm^2/second)		FA	
			Lesion	NAWM	Lesion	NAWM
Werring et al. (58)	1999	6/6	0.74–2.12	0.69–1.17	0.25–0.83	0.26–0.84
Tievsky et al. (59)	1999	12/NA	0.92–1.59	0.79	0.19–0.34	0.4
Bammer et al. (60)	2000	14/9	0.89–1.2	0.84	0.23–0.44	0.39–0.75
Filippi et al. (61)	2001	78/20	1.02–1.15	0.85–1.00	0.21–0.27	0.27–0.62
Ciccarelli et al. (62)	2001	39/21	NA	0.71–1.1	NA	0.53–0.76
Cercignani et al. (63)	2001	78/20	1.02	NA	0.19	NA
Iannucci et al. (64)	2001	34/15	0.66–1.11	NA	0.19–0.34	NA
Guo et al. (65)	2001	12/NA	0.90	0.76	0.30	0.462
Guo et al. (66)	2002	25/26	1.03	0.74	0.28	0.49
Rovaris et al. (67)	2002	96/44	0.99–1.04	0.85–0.87	0.19–0.2	NA

N = numbers of patients, MD = mean diffusivity; FA = fractional anisotropy; NAWM = normal appearing white matter; NA = not available.

ogy for temporal lobe epilepsy. MRI is sensitive in identifying mesial temporal sclerosis, with characteristic findings including hippocampal volume loss and T2 signal hyperintensity (71,72), but in some patients, it is difficult to identify the subtle abnormalities with conventional MR images.

DTI has been recently used in depicting abnormalities in patients with epilepsy. Increased diffusivity and reduced anisotropy in the sclerotic hippocampi of patients with chronic epilepsy and hippocampal sclerosis (73–75) (Fig. 11) suggest the loss of structural organization and expansion of the extracellular space. In patients with malformations of cortical development (MCD), another common association with refractory epilepsy, higher diffusivity and lower anisotropy were demonstrated not only within MCD (76), but also in areas that appeared normal on conventional MRI (76). In addition, these changes in diffusivity and anisotropy

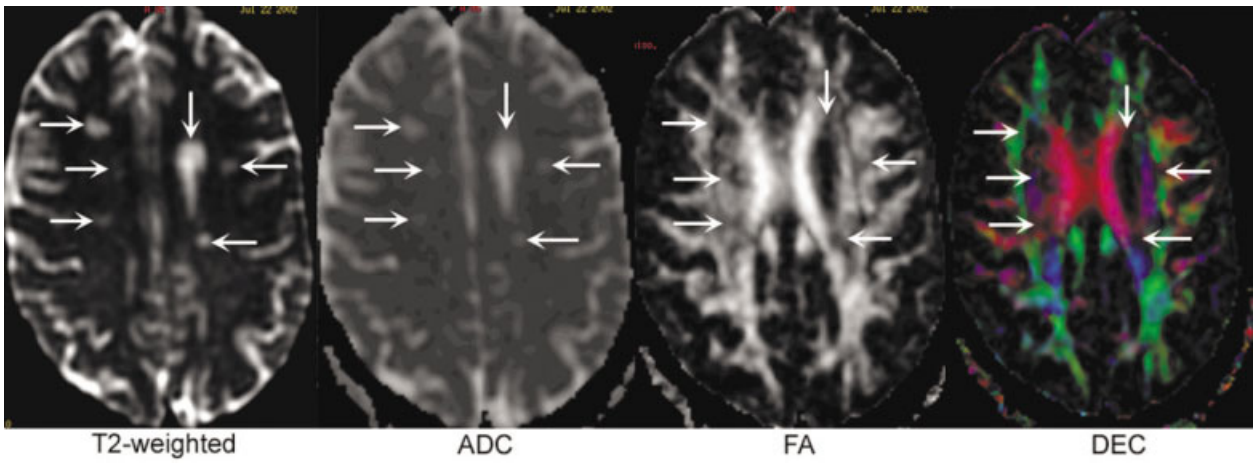

Figure 10. Axial images obtained from a 35-year-old female with MS. Multiple lesions are revealed in the T2-weighted image (arrows). On the ADC map, lesions appear as hyperintense compared with the surrounding tissue (increased ADC values). On the FA map and DEC images, lesions appear as dark areas within the white matter and have decreased FA values.

revealed in normal-appearing brain tissue beyond the origin of seizures have also been reported in other studies (75,77,78). This may be important to help localize lesions in MRI-negative patients and provide more information in detecting occult epileptogenic regions, offering possible surgical treatment for these individuals.

Metabolic Disorders

This group encompasses a wide spectrum of inherited neurodegenerative disorders that affect the gray and white matter to varying degrees. Leukodystrophies are the major classified diseases characterized by symmetric and diffuse white matter changes. They can be subdivided into lysosomal, peroxisomal, and mitochondrial diseases (79). Based on the advantage of the DTI technique in the assessment of white matter disease, several studies have been done to evaluate abnormalities related to demyelination in patients with adrenoleukodystrophy (ALD) (80,81) and Krabbe disease (82).

X-linked ALD is a rare, genetic disorder characterized by the breakdown or loss of the myelin sheath surrounding nerve cells in the brain and progressive dysfunction of the adrenal gland. A drop in FA and the increase in ADC were demonstrated by Eichler et al (81). The changes in ADC and FA values within the affected white matter from periphery to core correlate to histopathological zonal changes described by Schaumburg et al (83), which may indicate an increase in free water and loss of the integrity of the myelin sheath and axon in white matter (Fig. 12). Better sensitivity of anisotropy maps compared with conventional MRI in detecting dysmyelination in patients with Krabbe disease has been illustrated by early disease detection and by the correlation of treatment effects with alterations in anisotropic disturbances (82). Moreover, Ono et al (84,85) have found that DTI is superior to conventional MRI in differentiating dysmyelinating disorders (i.e., Pelizaeus-Merzbacher disease) from demyelinating disorders (i.e., Krabbe disease, Alexander disease). The existence of diffusional anisotropy in dysmyelinated lesions and the lack of diffusional anisotropy in demyelinated lesions has been verified in both animal and human studies (84,85).

Brain Tumor

Brain tumors are responsible for significant morbidity and mortality in both pediatric and adult populations. Approximately 18,000 brain tumors are diagnosed annually in the United States (86). Despite the information provided by conventional MR with contrast-enhanced T1-weighted and T2-weighted sequences in characterizing the location and extent of these tumors, the specification and grading of brain tumors is still limited. Diffusion imaging has been increasingly used

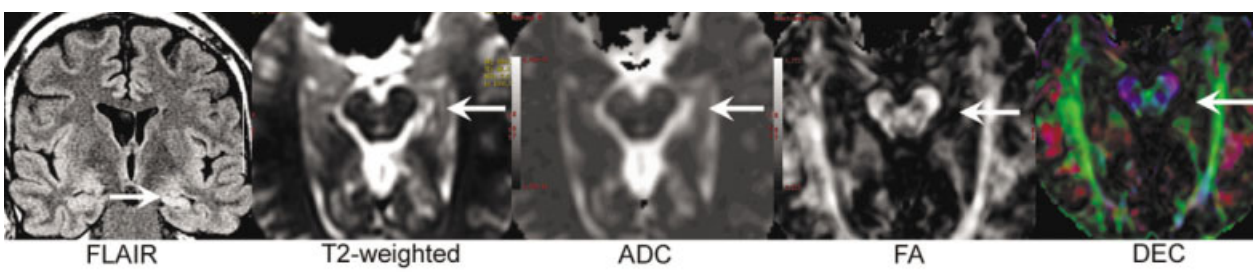

Figure 11. MR images from a 39-year-old right-handed male patient with refractory complex partial seizures. FLAIR and T2-weighted images show that the left hippocampus is atrophic with high signal (arrows) compared to the right side, suggesting left mesial temporal sclerosis. Hyperintensity with a significantly increased ADC value of 1.42×10^{-9} mm^2/second and hypointensity with a decreased FA value of 0.147 are demonstrated respectively in the ADC and FA maps.

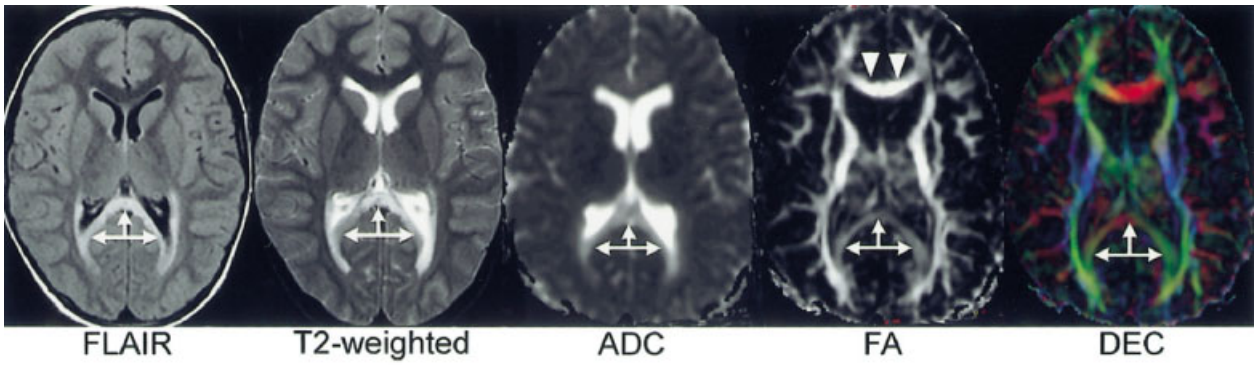

Figure 12. An eight-year-old boy with X-linked adrenoleukodystrophy. Hyperintense signal on T2- and FLAIR-weighted images along the splenium of the corpus callosum bilaterally, extends into the peritrigonal white matter of both occipital lobes (arrows). There is markedly increased ADC and decreased FA values. The FA map shows that the splenium of the corpus callosum is dark (arrows) compared with the genus of the corpus callosum (arrowheads). The splenium of the corpus callosum has lost its left to right fiber orientation, which also shown on DEC image.

Table 2
MD and FA Values in Tumor Studies

Reference	Year	*N*	MD ($\times 10^{-9}$ mm^2/second)			FA				
			Enhancing tumor	Nonenhancing tumor	Edema	NAWM	Enhancing tumor	Nonenhancing tumor	Edema	NAWM
Brunberg et al. (87)	1995	40	1.31	1.43	1.38	0.83	0.15	0.16	0.26	0.45
Krabbe et al. (88)	1997	12	1.37	NA	1.91	NA	NA	NA	NA	NA
Castillo et al. (89)	2001	15	1.31	NA	1.29	0.78	NA	NA	NA	NA
Stadnik et al. (90)	2001	11	1.14	NA	NA	0.66	NA	NA	NA	NA
Kono et al. (91)	2001	9/8[a]	0.82/1.14[a]	NA	1.42/1.38[a]	NA	NA	NA	NA	NA
Guo et al. (92)	2002	17	1.21	NA	NA	0.72	NA	NA	NA	NA
Sinha et al. (93)	2002	9	1.31	1.83	1.41	0.73	0.13	0.09	0.17	0.48
Bastin et al. (94)	2002	6	1.37	1.99	1.51	0.74	0.16	0.1	0.16	0.48

[a]Glioblastoma/grade II astrocytoma.
N = numbers of patients, MD = mean diffusivity, FA = fractional anisotropy, NAWM = normal appearing white matter, NA = not available.

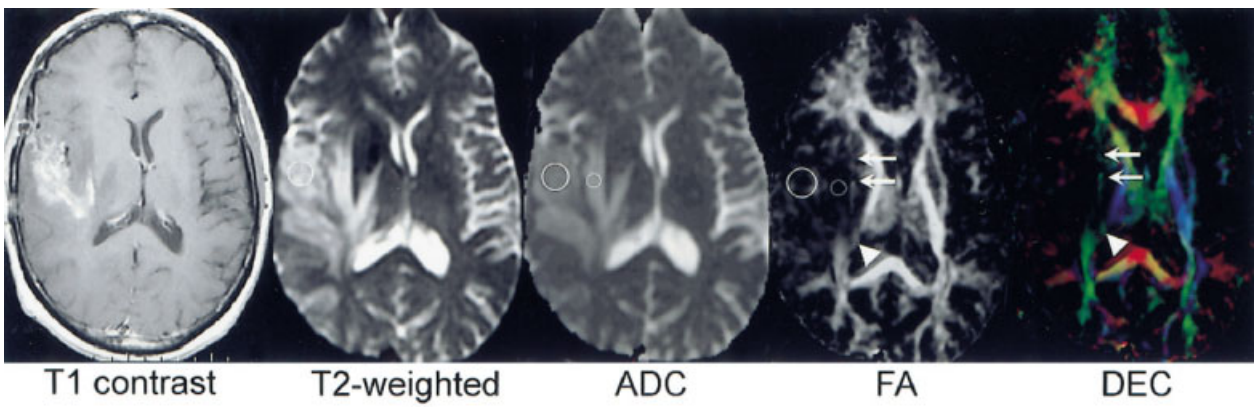

Figure 13. A 53-year-old male with glioblastoma multiforme postradiation/chemotherapy. The contrast-enhancing mass with extended edema peripherally is identified on axial T2- and contrast-enhanced T1-weighted images. The ADC map shows hyperintense signals for both tumor and edema; corresponding regions of interest (ROIs) were placed in enhanced tumor and edema regions. The ADC value for edema (1.68×10^{-9} mm^2/second) is higher than that for tumor (1.28×10^{-9} mm^2/second). Decreased FA is also demonstrated, with damaged external capsule (arrows) and posterior limb of the internal capsule (arrowhead) on the FA map, as well as on the DEC image.

to investigate various tumor components and assess tumoral invasion from normal tissue or edema. In several recent studies (87–94), ADC maps have been shown to be helpful in recognizing solid enhancing tumor and nonenhancing tumor, peritumoral edema, necrotic and cystic regions, and normal white matter (Table 2). Cystic or necrotic areas have the highest ADC values (87) and contrast-enhancing tumors have lower ADC values than both cystic or necrotic areas and edema (87–94).

Some have studied the correlation of ADC values with tumor type and grade (89,91,92,95): low-grade astrocy-

toma has higher ADC values, whereas high-grade malignant glioma has lower ADC values, reflecting more restricted diffusion from increasing tumor cellularity. FA values are generally reduced in the tumor, which suggests structural disorder, and may not be able to provide extra information in tissue differentiation (93). However, disorganization of the white matter tracts and the effects of tumor on white matter pathways can be identified with this value (Fig. 13) (96), which can not obtained with standard MR techniques. Understanding the tumor effect on white matter fibers may be important in neurosurgical planning. Data obtained from both animal models and human studies suggest that diffusion imaging may be sensitive for evaluating tumor response to therapy (97–100). Early increasing ADC values during therapy may relate to therapy-induced cell necrosis. The subsequent drop in tumor ADC to pretreatment levels is an indicator of tumor regrowth.

SUMMARY

DTI provides a powerful noninvasive tool to study complex brain tissue architecture. Its value in application to normal issues such as neuroanatomy, fiber connectivity, and brain development is promising. In addition, it also has tremendous potential in a broad variety of pathologies, such as cerebral ischemia, multiple sclerosis, epilepsy, metabolic disorders, and brain tumor. Advances in efficient MR acquisitions and suitable postprocessing algorithms are needed to further enhance the information derived from DTI. With technical improvements and robust postprocessing analyses, the utilization of DTI may become more reliable, both for research and clinical applications.

ACKNOWLEDGMENTS

We thank Suzanne Murphy for assistance with preparation of the manuscript.

REFERENCES

1. Le Bihan D, Breton E, Lallemand D, Grenier P, Cabanis E, Laval-Jeantet M. MR imaging of intravoxel incoherent motions: application to diffusion and perfusion in neurologic disorders. Radiology 1986;161:401–407.
2. Chenevert TL, Brunberg JA, Pipe JG. Anisotropic diffusion in human white matter: demonstration with MR techniques in vivo. Radiology 1990;177:401–405.
3. Pierpaoli C, Jezzard P, Basser PJ, Barnett A, Di Chiro G. Diffusion tensor MR imaging of the human brain. Radiology 1996;201:637–648.
4. Pajevic S, Pierpaoli C. Color schemes to represent the orientation of anisotropic tissues from diffusion tensor data: application to white matter fiber tract mapping in the human brain. Magn Reson Med 1999;42:526–540.
5. Brown R. A brief account of microscopical observations and on the general existence of active molecules in organic and inorganic bodies. In: The Philosophical Magazine, vol. IV. London: Richard Taylor; 1828. p 161–173.
6. Einstein A. About the movement of suspended particles in liquids at rest as required by the molecular kinetic theory of heat. [Uber die von der molekularkinetischen Theorie der Warme geforderte Bewegung von in ruhenden Flussigkeiten suspendierten Teilchen]. Ann Phys 1905;322:549–560. (Ger)
7. Crank J. The mathematics of diffusion. Oxford: Oxford University Press; 1975. p 1–10.
8. Callaghan P. Principles of nuclear magnetic resonance microscopy. Oxford: Oxford Science Publications; 1991. p 334–335.
9. Basser P, Mattiello J, LeBihan D. Estimation of the effective self-diffusion tensor from NMR spin echo. J Magn Reson B 1994;103: 247–254.
10. Stejskal E, Tanner J. Spin diffusion measurements: spin echoes in the presence of time-dependent field gradient. J Chem Phys 1965; 42:282–292.
11. Mattiello J, Basser P, Le Bihan D. The b matrix in diffusion tensor echo-planar imaging. Magn Reson Med 1997;37:292–300.
12. Mattiello J, Basser P, Lebihan D. Analytical expressions for the b matrix in NMR diffusion imaging and spectroscopy. J Magn Reson A 1994;108:131–141.
13. Basser P, Pierpaoli C. A simplified method to measure the diffusion tensor from seven MR images. Magn Reson Med 1998;39: 928–934.
14. Bammer R, Glover G, Moseley M. Diffusion tensor spiral imaging (abstract). In: Proceedings of the 10th Annual Meeting of the ISMRM, Honolulu, 2002;1111.
15. Ordidge R, Helpern J, Qing Z, Knight R, Nagesh V. Correction of motional artifacts in diffusion-weighted MR images using navigator echoes. Magn Reson Imag 1994;2:455–460.
16. Anderson A, Gore J. Analysis and correction of motion artifacts in diffusion weighted imaging. Magn Reson Med 1994;32:379–387.
17. Haacke E, Brown R, Thompson M, Venkatesan R. In chapter 19: Magnetic resonance imaging, physical principles and sequence design. New York: John Wiley & Sons, Inc.; 1999. p 513–567.
18. Pipe J, Farthing V, Forbes K. Multishot diffusion-weighted FSE using PROPELLER MRI. Magn Reson Med 2002;47:42–52.
19. Bammer R, Auer M, Keeling S, et al. Diffusion tensor imaging using single-shot SENSE-EPI. Magn Reson Med 2002;48:128–136.
20. Jones D, Horsfield M, Simmons A. Optimal strategies for measuring diffusion anisotropic systems by magnetic resonance imaging. Magn Reson Med 1999;42:515–525.
21. Skare S, Hedehus M, Moseley M, Li T. Condition number as a measure of noise performance of diffusion tensor acquisition schemes with MRI. J Magn Reson A 2000;147:340–352.
22. Reese T, Weisskoff R, Wedeen V. Diffusion NMR facilitated by a refocused eddy-current EPI pulse sequence (Abstract). In: Proceedings of the 6th Annual Meeting of the ISMRM, Sydney, Australia, 1998;663.
23. Papadakis N, Martin K, Pickard J, Hall L, Carpenter T, Huang C. Gradient preemphasis calibration in diffusion-weighted echo-planar imaging. Magn Reson Med 2000;44:616–624.
24. Basser P, Pierpaoli C. Microstructural and physiological features of tissues elucidated by quantitative-diffusion-tensor MRI. J Magn Reson B 1996;111:209–219.
25. Conturo T, Lori N, Cull T, et al. Tracking neuronal fiber pathways in the living human brain. Proc Natl Acad Sci USA 1999;96: 10422–10427.
26. Basser P, Pajevic S, Pierpaoli C, Duda J, Aldroubi A. In vivo fiber tractography using DT-MRI data. Magn Reson Med 2000;44:625–632.
27. Mori S, Van Zijl P. Fiber tracking: principles and strategies - a technical review. NMR Biomed 2002;15:468–480.
28. Tuch D, Weisskoff R, Belliveau J, Wedeen V. High angular resolution diffusion imaging of the human brain sequence (abstract). In: Proceedings of the 7th Annual Meeting of the ISMRM, Philadelphia, 1999;321.
29. Frank L. Anisotropy in high angular resolution diffusion-weighted MRI. Magn Reson Med 2001;45:935–939.
30. Frank L. Characterization of anisotropy in high angular resolution diffusion-weighted MRI. Magn Reson Med 2002;47:1083–1099.
31. Wedeen V, Reese T, Tuch D, et al. Mapping fiber orientation spectra in cerebral white matter with Fourier-transform diffusion MRI (abstract). In: Proceedings of the 8th Annual Meeting of the ISMRM, Denver, 2000;82.
32. Huppi P, Maier S, Peled S, et al. Microstructural development of human newborn cerebral white matter assessed in vivo by diffusion tensor magnetic resonance imaging. Pediatr Res 1998;44: 584–590.
33. Neil J, Shiran S, McKinstry R, et al. Normal brain in human newborns: apparent diffusion coefficient and diffusion anisotropy measured by using diffusion tensor MR imaging. Radiology 1998; 209:57–66.
34. McGraw P, Liang L, Provenzale J. Evaluation of normal age-related changes in anisotropy during infancy and childhood as shown by diffusion tensor imaging. AJR Am J Roentgenol 2002;179:1515–1522.

35. Mukherjee P, Miller J, Shimony J, et al. Normal brain maturation during childhood: developmental trends characterized with diffusion-tensor MR imaging. Radiology 2001;221:349–358.
36. Miller S, Vigneron D, Henry R, et al. Serial quantitative diffusion tensor MRI of the premature brain: development in newborns with and without injury. J Magn Reson Imaging 2002;16:621–632.
37. Pfefferbaum A, Sullivan E, Hedehus M, Lim K, Adalsteinsson E, Moseley M. Age-related decline in brain white matter anisotropy measured with spatially corrected echo-planar diffusion tensor imaging. Magn Reson Med 2000;44:259–268.
38. Sullivan E, Adalsteinsson E, Hedehus M, et al. Equivalent disruption of regional white matter microstructure in ageing healthy men and women. Neuroreport 2001;12:99–104.
39. Nusbaum A, Tang C, Buchsbaum M, Wei T. Atlas SW. Regional and global changes in cerebral diffusion with normal aging. AJNR Am J Neuroradiol 2001;22:136–142.
40. Gideon P, Thomsen C, Henriksen O. Increased self-diffusion of brain water in normal aging. Magn Reson Imaging 1994;4:185–188.
41. Astrup J, Symon L, Branston N, et al. Cortical evoked potential and extracellular K+ and H+ at critical levels of brain ischemia. Stroke 1997;8:51–57.
42. Moseley M, Kucharczyk J, Mintorovitch J, et al. Diffusion-weighted MR imaging of acute stroke: correlation with T2-weighted and magnetic susceptibility-enhanced MR imaging in cats. AJNR Am J Neuroradiol 1990;11:423–429.
43. Warach S, Chien D, Li W, Ronthal M, Edelman R. Fast magnetic resonance diffusion-weighted imaging of acute human stroke. Neurology 1992;42:1717–1723.
44. Ricci P, Burdette J, Elster A, Reboussin D. A comparison of fast spin echo, fluid-attenuated inversion-recovery, and diffusion-weighted MR imaging in the first 10 days after cerebral infarction. AJNR Am J Neuroradiol 1999;20:1535–1542.
45. Moseley M, Cohen Y, Mintorovitch J, et al. Early detection of regional cerebral ischemia in cats: comparison of diffusion - and T2-weighted MRI and spectroscopy. Magn Reson Med 1990;14: 330–346.
46. Sorensen A, Buonanno F, Gonzalez R, et al. Hyperacute stroke: evaluation with combined multisection diffusion-weighted and hemodynamically weighted echo-planar MR imaging. Radiology 1996;199:391–401.
47. Schlaug G, Siewert B, Benfield A, Edelman R, Warach S. Time course of the apparent diffusion coefficient (ADC) abnormality in human stroke. Neurology 1997;49:113–119.
48. Yamada N, Imakita S, Sakuma T. Value of diffusion-weighted imaging and apparent diffusion coefficient in recent cerebral infarctions: a correlative study with contrast-enhanced T1-weighted imaging. AJNR Am J Neuroradiol 1999;20:193–198.
49. Zelaya F, Flood N, Chalk J, et al. An evaluation of the time dependence of the anisotropy of the water diffusion tensor in acute human ischemia. Magn Reson Imaging 1999;17:331–348.
50. Mukherjee P, Bahn M, McKinstry R, et al. Differences between gray matter and white matter diffusion in stroke: diffusion-tensor MR imaging in 12 patients. Radiology 2000;215:211–220.
51. Sorensen A, Wu O, Copen W, et al. Human acute cerebral ischemia: detection of changes in water diffusion anisotropy by using MR imaging. Radiology 1999;212.
52. Kuhn M, Mikulis D, Ayoub D, Kosofsky B, Davis K, Taveras J. Wallerian degeneration after cerebral infarction: evaluation with sequential MR imaging. Radiology 1989;172:179–182.
53. Castillo M, Mukherji S. Early abnormalities related to postinfarction Wallerian degeneration: evaluation with MR diffusion-weighted imaging. J Comput Assist Tomogr 1999;23:1004–1007.
54. Wieshmann U, Symms M, Clark C, et al. Wallerian degeneration in the optic radiation after temporal lobectomy demonstrated in vivo with diffusion tensor imaging. Epilepsia 1999;40:1155–1158.
55. Werring D, Toosy A, Clark C, et al. Diffusion tensor imaging can detect and quantify corticospinal tract degeneration after stroke. J Neurol Neurosurg Psychiatry 2000;69:269–272.
56. Pierpaoli C, Barnett A, Pajevic S. Water diffusion changes in Wallerian Degeneration and their dependence on white matter architecture. Neuroimage 2001;13:1174–1185.
57. Miller D, Grossman R, Reingold S, Mcfarland H. The role of magnetic resonance techniques in understanding and managing multiple sclerosis. Brain 1998;121:3–24.
58. Werring D, Clark C, Barker G, et al. Diffusion tensor imaging of lesions and normal-appearing white matter in multiple sclerosis. Neurology 1999;52:1626–1632.
59. Tievsky A, Ptak T, Farkas J. Investigation of apparent diffusion coefficient and diffusion tensor anisotropy in acute and chronic multiple sclerosis lesions. AJNR Am J Neuroradiol 1999;20:1491–1499.
60. Bammer R, Augustin M, Strasser-Fuchs S, et al. Magnetic resonance diffusion tensor imaging for characterizing diffuse and focal white matter abnormalities in multiple sclerosis. Magn Reson Med 2000;44:583–591.
61. Filippi M, Cercignani M, Inglese M, Horsfield M, Comi G. Diffusion tensor magnetic resonance imaging in multiple sclerosis. Neurology 2001;56:304–311.
62. Ciccarelli O, Werring D, Wheeler-Kingshott C, et al. Investigation of MS normal-appearing brain using diffusion tensor MRI with clinical correlations. Neurology 2001;56:926–933.
63. Cercignani M, Inglese M, Pagani E, Comi G, Filippi M. Mean diffusivity and fractional anisotropy histograms of patients with multiple sclerosis. AJNR Am J Neuroradiol 2001;22:952–958.
64. Iannucci G, Rovaris M, Giacomotti L, Comi G, Filippi M. Correlation of multiple sclerosis measures derived from T2-weighted, T1-weighted, magnetization transfer, and diffusion tensor MR imaging. AJNR Am J Neuroradiol 2001;22:1462–1467.
65. Guo A, Jewells V, Provenzale J. Analysis of normal-appearing white matter in multiple sclerosis: comparison of diffusion tensor MR imaging and magnetization transfer imaging. AJNR Am J Neuroradiol 2001;22:1893–1900.
66. Guo A, MacFall J, Provenzale J. Multiple sclerosis: diffusion tensor MR imaging for evaluation of normal-appearing white matter. Radiology 2002;222:729–736.
67. Rovaris M, Bozzali M, Iannucci G, et al. Assessment of normal-appearing white and gray matter in patients with primary progressive multiple sclerosis: a diffusion-tensor magnetic resonance imaging study. Arch Neurol 2002;59:1406–1412.
68. Bozzali M, Cercignani M, Sormani M, Comi G, Filippi M. Quantification of brain gray matter damage in different MS phenotypes by use of diffusion tensor MR imaging. AJNR Am J Neuroradiol 2002;23:985–988.
69. Cercignani M, Bozzali M, Iannucci G, Comi G, Filippi M. Intravoxel and inter-voxel coherence in patients with multiple sclerosis assessed using diffusion tensor MRI. J Neurol 2002;249:875–883.
70. Engel J Jr, Shewmon D. Overview: who should be considered a surgical candidate? In Engel J Jr, editor. Surgical treatment of the epilepsies. 2nd edition. New York: Raven Press, 1993; p 23–24.
71. Brooks B, King D, Gammal T, et al. MR imaging in patients with intractable complex partial epileptic seizures. AJNR Am J Neuroradiol 1990;11:93–99.
72. Tien R, Felsberg G, Castro C, et al. Complex partial seizure and mesial temporal sclerosis: evaluation with fast spin-echo MR imaging. Radiology 1993;189:835–842.
73. Hugg J, Butterworth E, Kuzniecky R. Diffusion mapping applied to mesial temporal lobe epilepsy. Preliminary observation. Neurology 1999;53:173–176.
74. Wieshmann U, Clark C, Symms M, Barker G, Birnie K, Shorvon S. Water diffusion in the human hippocampus in epilepsy. Magn Reson Imaging 1999;17:29–36.
75. Yoo S, Chang K, Song I, et al. Apparent diffusion coefficient value of the hippocampus in patients with hippocampal sclerosis and in healthy volunteers. AJNR Am J Neuroradiol 2002;23:809–812.
76. Eriksson S, Rugg-Gunn F, Symms M, Barker G, Duncan J. Diffusion tensor imaging in patients with epilepsy and malformations of cortical development. Brain 2001;124:617–626.
77. Fugg-Gunn F, Eriksson S, Symms M, et al. Diffusion tensor imaging of cryptogenic and acquired partial epilepsies. Brain 2001; 124:627–636.
78. Arfanakis K, Hermann B, Rogers B, Carew J, Seidenberg M, Meyerand M. Diffusion tensor MRI in temporal lobe epilepsy. Magn Reson Imaging 2002;20:511–519.
79. Kendall B. Disorders of lysosomes, peroxisomes, and mitochondria. AJNR Am J Neuroradiol 1992;13:621–653.
80. Ito R, Melhem E, Mori S, Eichler F, Raymond G, Moser H. Diffusion tensor brain MR imaging in X-linked cerebral adrenoleukodystrophy. Neurology 2001;56:544–547.
81. Eichler F, Itoh R, Barker P, et al. Proton MR spectroscopic and diffusion tensor brain MR imaging in X-linked adrenoleukodystrophy: initial experience. Radiology 2002;225:245–252.

82. Guo A, Petrella J, Kurtzberg J, et al. Evaluation of white matter anisotropy in Krabbe disease with diffusion tensor MR imaging: initial experience. Radiology 2001;218:809–815.
83. Schaumburg H, Powers J, Raine C, Suzuki K, Richardson E. Adrenoleukodystrophy: a clinical and pathological study of 17 cases. Arch Neurol 1975;32:577–591.
84. Ono J, Harada K, Takahashi M, et al. Differentiation between dysmyelination and demyelination using magnetic resonance diffusional anisotropy. Brain Res 1995;671:141–148.
85. Ono J, Harada K, Mano T, Sakurai K, Okada S. Differentiation of dys- and demyelination using diffusional anisotropy. Pediatr Neurol 1997;16:63–66.
86. Legler J, Ries L, Smith M, et al. Cancer surveillance series [corrected]: brain and other central nervous system cancers: recent trends in incidence and mortality. J Natl Cancer Inst 1999;91: 1382–1390.
87. Brunberg J, Chenevert T, McKeever P, et al. In vivo MR determination of water diffusion coefficients and diffusion anisotropy: correlation with structural alteration in gliomas of the cerebral hemispheres. AJNR Am J Neuroradiol 1995;16:361–371.
88. Krabbe K, Gideon P, Wagn P, Hansen U, Thomsen C, Madsen F. MR diffusion imaging of human intracranial tumors. Neuroradiology 1997;39:483–489.
89. Castillo M, Smith J, Kwock L, Wilber K. Apparent diffusion coefficients in the evaluation of high-grade cerebral gliomas. AJNR Am J Neuroradiol 2001;22:60–64.
90. Stadnik T, Chaskis C, Michotte A, et al. Diffusion-weighted MR imaging of intracerebral masses: comparison with conventional MR imaging and histologic findings. AJNR Am J Neuroradiol 2001; 22:969–976.
91. Kono K, Inoue Y, Nakayama K, et al. The role of diffusion-weighted imaging in patients with brain tumors. AJNR Am J Neuroradiol 2001;22:1081–1088.
92. Guo A, Cummings T, Dash R, Provenzale J. Lymphomas and high-grade astrocytomas: comparison of water diffusibility and histologic characteristics. Radiology 2002;224:177–183.
93. Sinha S, Bastin M, Whittle I, et al. Diffusion tensor MR imaging of high-grade cerebral gliomas. AJNR Am J Neuroradiol 2002;23: 520–527.
94. Bastin M, Sinha S, Whittle I, Wardlaw J. Measurements of water diffusion and T1 values in peritumoural oedematous brain. Neuroreport 2002;13:1335–1340.
95. Gauvain K, McKinstry R, Mukherjee P, et al. Evaluating pediatric brain tumor cellularity with diffusion-tensor imaging. AJR Am J Roentgenol 2001;177:449–454.
96. Mori S, Frederiksen K, van Zijl P, et al. Brain white matter anatomy of tumor patients evaluated with diffusion tensor imaging. Ann Neurol 2002;51:377–380.
97. Chenevert T, McKeever P, Ross B. Monitoring early response of experimental brain tumors to therapy using diffusion magnetic resonance imaging. Clin Cancer Res 1997;3:1457–1466.
98. Chenevert T, Stegman L, Taylor J, et al. Diffusion magnetic resonance imaging: an early surrogate marker of therapeutic efficacy in brain tumors. J Natl Cancer Inst 2000;92:2029–2036.
99. Mardor Y, Pfeffer R, Spiegelmann R, et al. Early detection of response to radiation therapy in patients with brain malignancies using conventional and high b-value diffusion-weighted magnetic resonance imaging. J Clin Oncol 2003;21:1094–1100.
100. Dzik-Jurasz A, Domenig C, George M, et al. Diffusion MRI for prediction of response of rectal cancer to chemoradiation. Lancet 2002;360:307–308.